Behavior of Forging Steels under Cyclic Loading—the Benefit of Air-Hardening Martensites

Tobias Schmiedl,* Alexander R. M. Gramlich, Steffen Schönborn, and Tobias Melz

The development of air-hardening martensitic forging (LHD: luft härtend duktil) steels offers high material performance with a short and simple process route. In this study, five alloys (L1–L5), based on the existing LHD alloy concept but with different contents of aluminum, titanium, boron, and molybdenum, are cast at laboratory scale. The casted blocks are hot forged into semifinished products and cooled in air (uncontrolled). The tensile properties, the Charpy V-notch impact energy, the cyclic material behavior, and the fatigue strength of the alloys L1–L5 are opposed to each other. Furthermore, the material properties are compared with the standard quench and tempered (Q+T) steel 42CrMo4 (reference material) and ranked against previously developed forging steels. The tensile properties and Charpy V-notch impact energy are comparable with those of the reference material, whereas the new alloy concepts show a significantly higher cyclic yield strength and fatigue strength.

1. Introduction

The reduction of CO_2-emissions is the most significant challenge for the future. A strong focus is being taken on achieving a CO_2-neutral transport sector. Different power unit systems with low emissions (battery electric vehicles, fuel cell electric vehicles, conventional vehicles with synthetic fuels, and compressed natural gas and hybrid vehicles) will coexist in the future transport sector. The replacement of fuel tanks by batteries and hydrogen tanks will significantly increase the weight of vehicles. A lightweight design is therefore necessary to increase the efficiency

T. Schmiedl, Prof. T. Melz
System Reliability, Adaptive Structures and Machine Acoustics SAM
Technical University of Darmstadt
Magdalenenstr. 4, 64289 Darmstadt, Germany
E-mail: tobias.schmiedl@sam.tu-darmstadt.de

A. R. M. Gramlich
Steel Institute
RWTH Aachen University
Intzestraße 1, 52072 Aachen, Germany

Dr. S. Schönborn, Prof. T. Melz
Structural Durability
Fraunhofer Institute for Structural Durability and System Reliability LBF
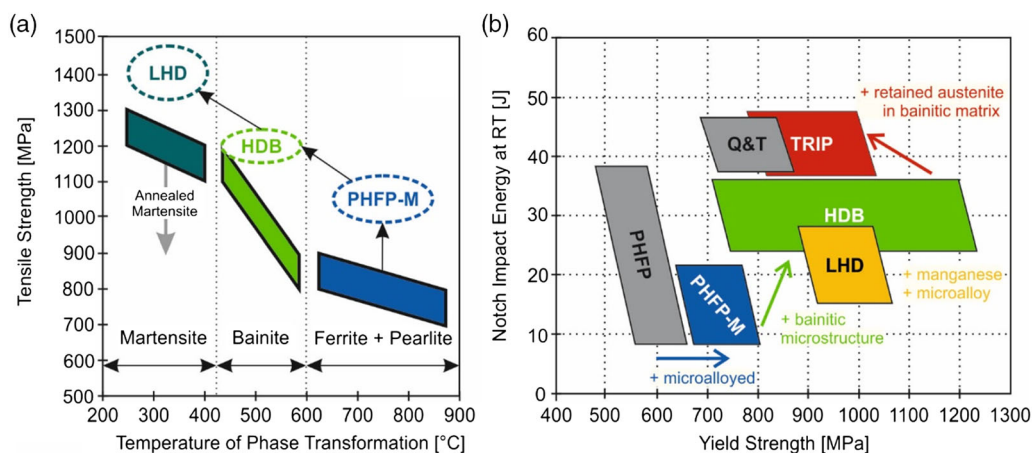Bartningstraße 47, 64289 Darmstadt, Germany

The ORCID identification number(s) for the author(s) of this article can be found under https://doi.org/10.1002/srin.202000172.

and range of electric vehicles and to maintain the competitiveness of vehicles with combustion engines. However, the industry must also reduce its own CO_2 pollution. Extensive heat treatments lead to CO_2-emissions and have to be reduced as much as possible, especially for steel production and the downstream processing (e.g., forging). Shorter process routes will become indispensable and will in addition lead to lower production costs. Therefore, this study shows the development of new cost-efficient forging steel concepts with the following requirements: 1) a short and simple process route without additional heat treatments after hot forging to reduce CO_2-emissions and 2) martensitic microstructure with high strength and increased fatigue properties in comparison to standard quench and tempered steel to enable lightweight design in future vehicles. Quench and tempered (Q+T) steels and precipitation-hardening ferritic–pearlitic (PHFP) steels are the state of the art in the forging industry. Q+T steels offer, through their martensitic microstructure, a good combination of high tensile properties and high Charpy V-notch impact energy.[1] However, additional heat treatments are necessary after hot forging to achieve these properties. In comparison, PHFP steels do not need additional heat treatments and achieve their ferritic–pearlitic microstructure by controlled cooling from the forging temperature. However, the tensile properties of PHFP steels do not reach the levels of Q+T steels.[2–6] Nevertheless, PHFP steels offer the potential for comparable fatigue strength in the high-cycle fatigue (HCF) regime in comparison to Q+T steels, which shows cyclic softening.[4,5] The strength of forging steels is mainly determined by the microstructural matrix (**Figure 1**a). However, the transformation temperature decreases from ferrite+pearlite over bainite to martensite (Figure 1a), leading to high demands on the process route after hot forging. For a short and simple process route, modifications of the alloy design focus on an increase of the strengthening mechanisms and on the adjustment of the transformation behavior by the chemical composition. This has led to the development of several new forging steel grades (Figure 1b). For PHFP steels, microalloying with niobium, titanium, vanadium, and aluminum leads to a higher amount of grain refinement and precipitation strengthening.[1] Therefore microalloyed precipitation strengthening ferritic–pearlitic (PHFP-M) steels show higher tensile properties than PHFP steels but the values of the Charpy V-notch impact energy still remain at a low level (Figure 1b).[9,10] High-strength ductile bainitic (HDB) steels were developed to match more closely the levels of

ADVANCED
SCIENCE NEWS
www.advancedsciencenews.com

steel
research
international
www.steel-research.de

Figure 1. a) Ultimate tensile strength versus temperature of phase transformation,[7] amended by LHD steels. b) Charpy V-notch impact energy at room temperature versus yield strength for different forging steels.[8]

Q+T steels. The carbide-free bainitic microstructure leads to high tensile properties and a high Charpy V-notch impact energy[7,11–13] (see Figure 1b). However, because of the low phase transformation temperature of the bainite (Figure 1a), isothermal cooling after hot- forging is necessary to achieve a fully bainitic microstructure. The HDB alloy concept has been further modified to contain a certain amount of retained austenite as a second phase. This leads to the increased fatigue strength of the so-called transformation-induced plasticity (TRIP) steels, due to a deformation-induced transformation of austenite to martensite.[14–16] Recently, the focus has been set on simplifying cooling conditions while maintaining high tensile properties. Air-hardening (LHD: luft härtend duktil) steels offer high strength, comparable with Q+T steels (Figure 1b), and an easy process route in common with PHFP steels.[17–19] By adding around 4 wt% manganese, a nearly fully martensitic microstructure is achieved by air cooling.[17–19] Unfortunately, manganese segregates to former austenite grain boundaries, leading to a low Charpy V-notch impact energy.[20] Alloying with boron[21,22] and/or molybdenum[23] seems to be a possible way to strengthen the grain boundaries and to increase the Charpy V-notch impact energy. Furthermore, decreasing the former austenite grain size is also an option for increasing the Charpy V-notch impact energy.[19]

2. Experimental Section

The new alloy concepts are compared with the Q+T steel 42CrMo4, which is therefore set as the reference steel and represents the maximum alloying costs. The development of the LHD steels led to the alloy LHD-11, which contains around 4 wt% manganese, 0.2 wt% carbon, and 0.5 wt% silicon (see **Table 1**). This manganese content successfully suppresses the diffusion-controlled transformations, whereas higher manganese content would lead to embrittlement.[18,19] Silicon is alloyed to avoid cementite formation.[18,19] Based on this concept, for the new developments the alloying elements niobium, boron, molybdenum, titanium, and aluminum were alloyed in different amounts to achieve a high Charpy V-notch impact energy and increased fatigue properties, resulting in five alloy concepts (Table 1). All alloys contain 0.035 wt% niobium for grain refinement of the prior austenite grain boundaries. For alloys L1 and L2, the amount of boron was varied to strengthen the grain boundaries and titanium content was adjusted to prevent the formation of boron nitrides (**Figure 2**). Alloy L3 contains no significant amounts of boron and titanium but was alloyed with molybdenum for grain boundary strengthening (Figure 2). L4 was alloyed with both boron and molybdenum; furthermore titanium was replaced by high amounts of aluminum (Figure 2).

Table 1. Chemical composition of the alloys. All concentrations are given in wt%.

Alloy	C	Si	Mn	P	S	Al	Cr	Mo	Ti	Nb	B	N
42CrMo4[16]	0.42	0.30	0.85	0.009	0.001	0.010	1.17	0.23	<0.003	<0.003	<0.0005	0.006
LHD-11[19]	0.21	0.52	4.03	0.010	0.010	0.026	0.11	0.02	0.033	–	0.0029	0.008
L1	0.19	0.50	4.02	0.008	0.011	0.031	0.11	0.02	0.020	0.035	0.0016	0.011
L2	0.17	0.50	3.99	0.010	0.009	0.025	0.11	0.02	0.020	0.033	0.0057	0.010
L3	0.15	0.49	4.02	0.011	0.009	0.027	0.12	0.20	<0.003	0.035	<0.0005	0.010
L4	0.16	0.52	4.00	0.010	0.010	0.510	0.11	0.20	<0.003	0.037	0.0030	0.011
L5	0.17	0.50	3.96	0.010	0.009	0.027	0.12	0.02	<0.003	0.032	<0.0005	0.011
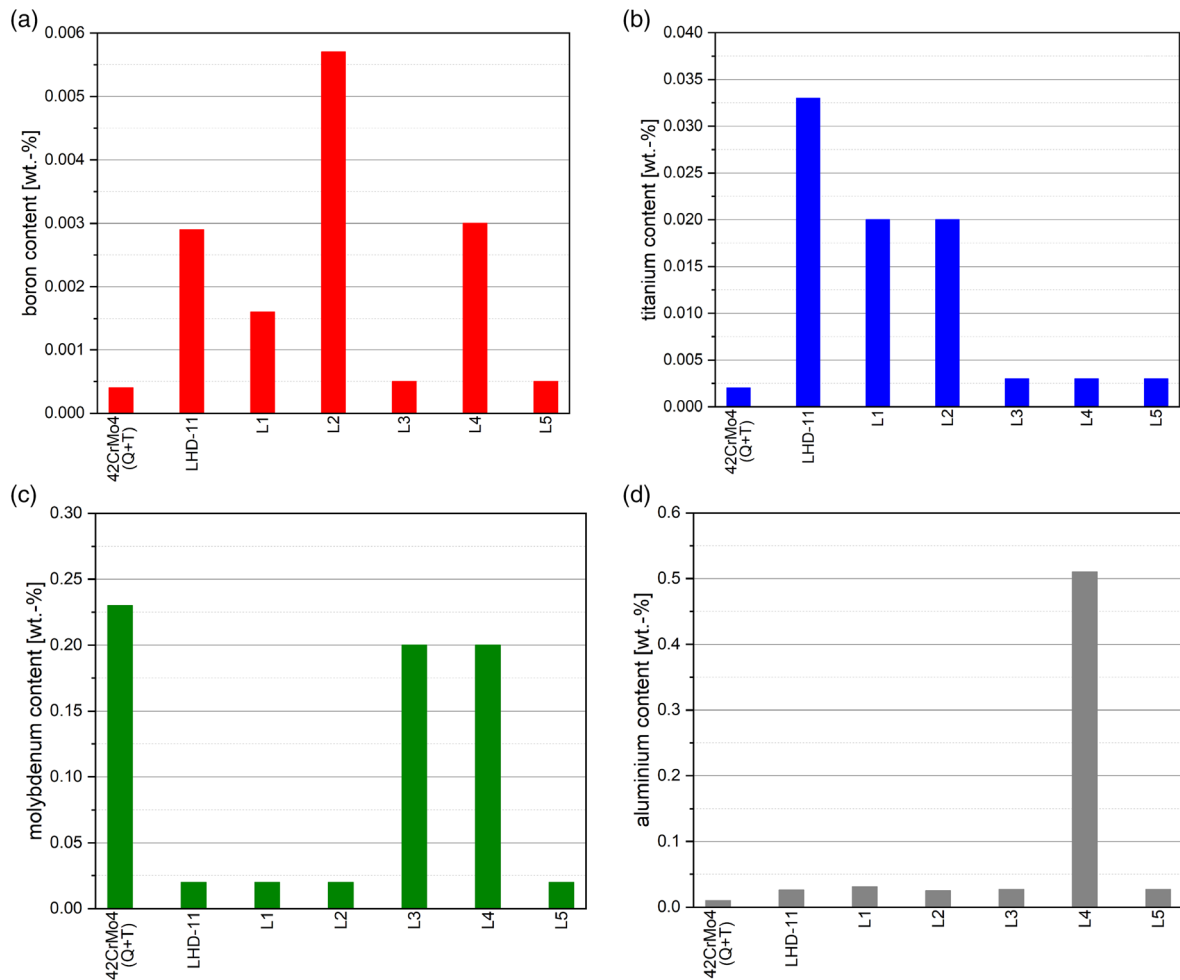
Figure 2. a) Boron, b) titanium, c) molybdenum, and d) aluminum contents for the Q+T steel 42CrMo4, LHD steel LHD-11, and the alloys L1–L5.
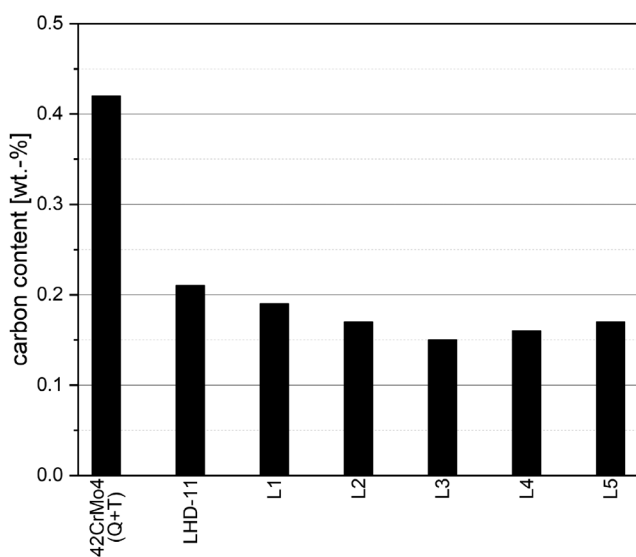
Figure 3. Carbon contents for the Q+T steel 42CrMo4, the LHD steel LHD-11, and the alloys L1–L5.

Alloy L5 contains no significant amounts of B, Ti, Mo, and Al. The carbon content of the alloys was also varied from 0.19 to 0.15 wt% (see **Figure 3**).

For all five alloys, a block was ingot cast at the Steel Institute using a laboratory-scale vacuum furnace. The Steel Institute of RWTH Aachen University is able to reproduce the hot-forging manufacturing process with their Semi Product Simulation Center (SPSC). Using the SPSC, each block was austenitized for 5 h at 1200 °C, then hot forged from $140 \times 140 \times 500$ mm^3 to $60 \times 60 \times 1000$ mm^3 in multiple steps and cooled in air (uncontrolled). The alloy LHD-11 was produced with the same procedure. For the Q+T steel 42CrMo4, a bloc of $130 \times 130 \times 100$ mm^3 was hardened for 72 min at 880 °C, cooled in oil to room temperature, annealed for 167 min, and cooled in air to room temperature.[16]

Samples for the characterization of material properties were taken from the transition between the center and edge of the blocks. Mechanical characterization was conducted through tensile tests according to DIN EN ISO 6892-1[24] and Charpy-V-notch tests at room temperature according to DIN EN ISO 14556.[25] The cyclic material behavior was investigated through incremental step tests (ISTs). ISTs represent strain-controlled fatigue tests

ADVANCED
SCIENCE NEWS
www.advancedsciencenews.com

steel
research
international
www.steel-research.de

Table 2. Specimen geometry and amount of tested specimen for the tensile tests, Charpy V-notch tests, ISTs, and SN-fatigue tests.

Tensile test (three specimens for each alloy)	Charpy V-notch test (three specimens for each alloy)

Incremental Step Test (two specimens for each alloy)	SN-fatigue test (six to nine specimens for each alloy)

with variable amplitudes on unnotched round specimens ($K_t = 1$) under alternating loading ($R_\varepsilon = -1$). The investigation of the fatigue strength in the low-cycle fatigue (LCF) and in the HCF regime was performed by load-controlled stress amplitude (SN, number of cycles to failure)-fatigue tests on notched specimens ($K_t = 2$) under tensile loading ($R_\sigma = 0$). The SN curves were evaluated with the maximum-likelihood method[26] and the fatigue strength was determined at $N = 1 \times 10^7$ cycles with a 50% probability of survivability. The specimen geometries and the amount of samples for each alloy can be extracted from **Table 2**. Further information regarding the setup for tensile, Charpy V-notch, and cyclic testing has been published in Schmiedl and Gramlich.[27] Unloaded portions of the Charpy V-notch and notched fatigue specimens were used for microstructural analysis. Nital etching was used for examination of the microstructure. The surfaces of the fractured notched fatigue specimens were analyzed by scanning electron microscopy, using a ZEISS Supra 25 and secondary electron detector with an acceleration voltage of 20 kV.

3. Results

3.1. Microstructure

Optical microscopy reveals a nearly fully martensitic microstructure for the alloys L1–L4 and a martensitic/bainitic microstructure for L5 (see **Figure 4**). The volume fraction of bainite increases, for all alloys, from the surface to the core of the forged

block. The prior austenite grain sizes for alloys L1–L5 are 27, 50, 59, 46, and 40 µm, respectively.[28] Several types of precipitates were found in the alloys L1–L5; a detailed microstructural investigation has been reported in Gramlich et al.[28] All five alloys contain carbides as well as manganese sulfides.[28] In addition, alloys L2 and L3 contain large titanium nitrides and alloy L4 contains aluminum nitrides.[28]

3.2. Tensile Properties

The reference steel 42CrMo4 shows a yield strength of 954 MPa and a tensile strength of 1090 MPa (**Figure 5**). The former LHD steel concept, LHD-11, has already led to a comparable yield strength (909 MPa) and to an increase by 430 MPa in tensile strength (1523 MPa), in comparison with the reference steel 42CrMo4 (Figure 5). The alloys L1–L5 show a yield strength in the range of 918–993 MPa and a tensile strength in the range 1340–1511 MPa (Figure 5). Both strength values decrease from alloy L1 to L4 and then increase for alloy L5. The alloy L5 shows almost an identical yield and tensile strength to L2 (Figure 5). The tensile properties of the new alloys are in the range of the alloy LHD-11, so the main advantage is a higher tensile strength in comparison with the reference steel 42CrMo4.

With reference to the ductility, the reference steel 42CrMo4 and the alloy LHD-11 show a uniform elongation of about 5.0% (see **Figure 6**). The alloys L1–L5 show a lower uniform elongation by around 1.0% (Figure 6). The elongations to fracture of the alloys L1–L5 and of the alloys LHD-11 are about 0.5% lower in
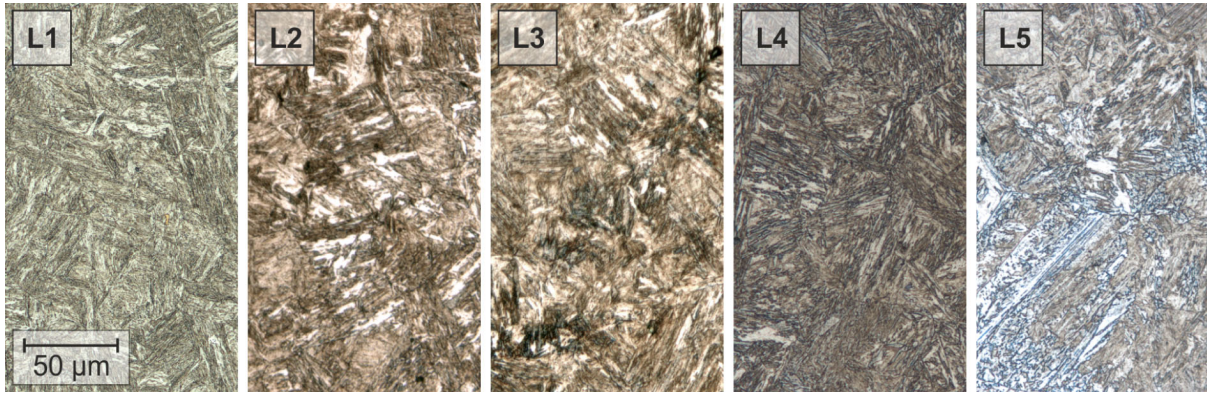
2000172 (4 of 10)

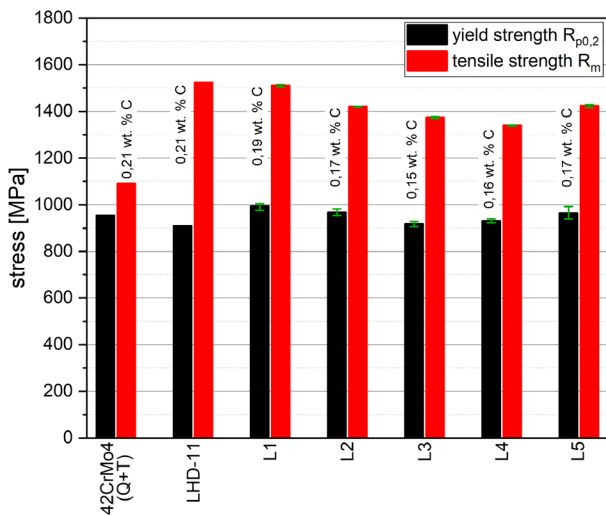**Figure 4.** Microstructures of the alloys L1–L5, revealed by nital etching.

Figure 5. Yield strength $R_{p0.2}$ and tensile strength R_m of the Q+T steel 42CrMo4,[16] the LHD steel LHD-11,[19] and the alloys L1–L5.[27]
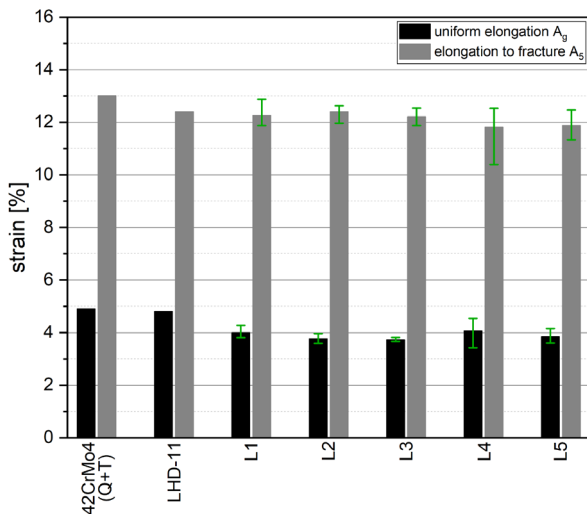
comparison with the reference steel 42CrMo4 (Figure 6). The new alloys offer a higher performance than the Q+T steel 42CrMo4 with respect to the tensile properties and the process route.

3.3. Charpy V-Notch Impact Energy at Room Temperature

The former LHD steel, LHD-11, reaches only a moderate Charpy V-notch impact energy of 29 J, whereas the reference steel 42CrMo4 shows a high Charpy V-notch impact energy of 51 J, see **Figure 7**. The Charpy V-notch impact energies of the alloys L1–L5 show a completely different trend than the tensile properties. Only alloy L4 shows a high Charpy V-notch impact energy comparable to the reference steel 42CrMo4 (Figure 7). The alloys L1, L3, and L5 show a relatively low Charpy V-notch impact energy of 11–16 J and L2 shows a moderate Charpy V-notch impact energy of 25 J (Figure 7).

3.4. Cyclic Material Behavior

ISTs provide the monotonic yield strength from the initial loading curve and the cyclic yield strength from the cyclic
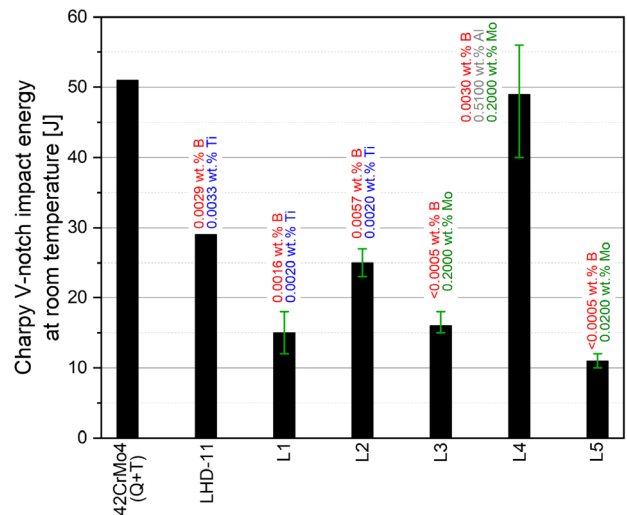

Figure 6. Uniform elongations A_g and elongations to fracture A_5 of the Q+T steel 42CrMo4,[16] the LHD steel LHD-11,[19] and the alloys L1–L5.[27]

Figure 7. Charpy V-notch impact energies at room temperature of the Q+T steel 42CrMo4,[16] the LHD steel LHD-11,[19] and the alloys L1–L5.[27]

stress–strain curve. Initial loading and cyclic stress–strain curves of the alloys L1–L5 have been shown elsewhere.[27] The comparison between the monotonic and the cyclic yield strength indicates the cyclic material behavior. If the cyclic yield strength is higher than the monotonic yield strength, cyclic hardening occurs and, if it is lower, cyclic softening takes place. A cyclically neutral material behavior appears if no significant difference exists between monotonic and cyclic yield strengths.

The standard Q+T steel 42CrMo4 shows a cyclic softening leading to a low cyclic yield strength of 560 MPa (see **Figure 8**). In contrast, the alloys L1–L5 show a cyclic hardening and the cyclic yield strengths of the alloys L1–L5 are about 70–90% higher than that of the Q+T steel 42CrMo4 (Figure 8). Analogous to the tensile strength, the cyclic yield strengths of the alloys decrease from L1 to L4 and then increase for L5 (Figure 8).

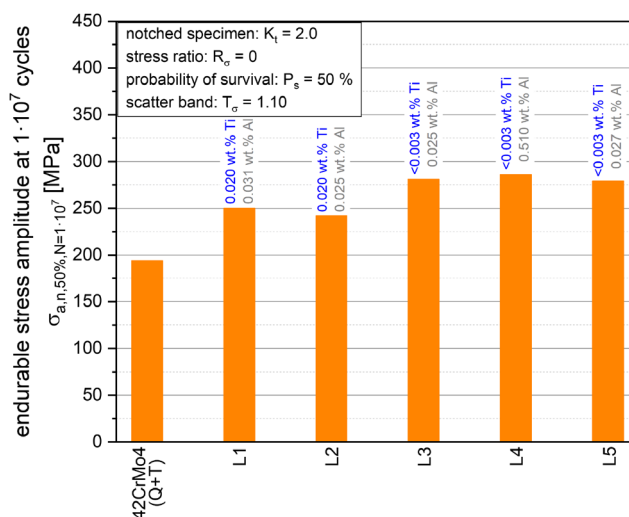### 3.5. Fatigue Strength of Notched Specimen in the HCF Regime

Spring clips, axles, and stub axles are typical forging components that are designed for long lifetime and are often loaded with tensile mean stresses. Therefore, a high fatigue strength in the HCF regime is necessary to perform a lightweight design. The Q+T steel 42CrMo4 shows a fatigue strength in the HCF regime of 194 MPa ($N = 1 \times 10^7$ cycles) (see **Figure 9**). The fatigue strengths in the HCF regime ($N = 1 \times 10^7$ cycles) of all the new alloys (L1–L5) are about 25–48% higher in comparison with the reference steel 42CrMo4 (Figure 9). The alloys L1 and L2, as well as L3–L5, show a comparable fatigue strength of 245 MPa and 280 MPa, respectively. The alloy L4 offers the best performance with a fatigue strength of 286 MPa (Figure 9).

3.6. Fatigue Fracture Behavior

Fractographic analyses of the notched fatigue specimens were performed to identify the influence of the alloying elements on the crack initiation and propagation behavior. Therefore,
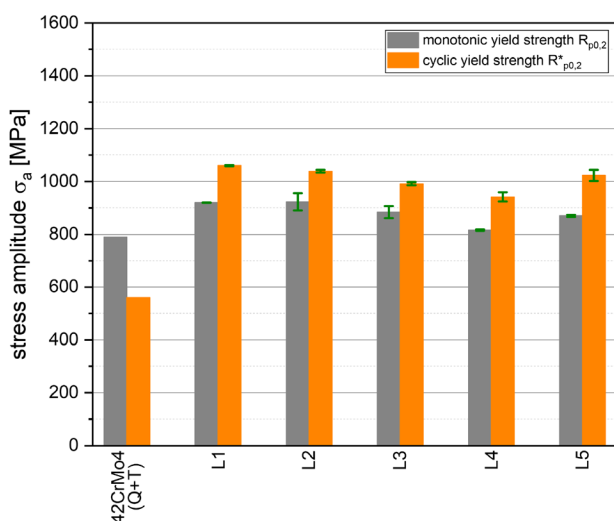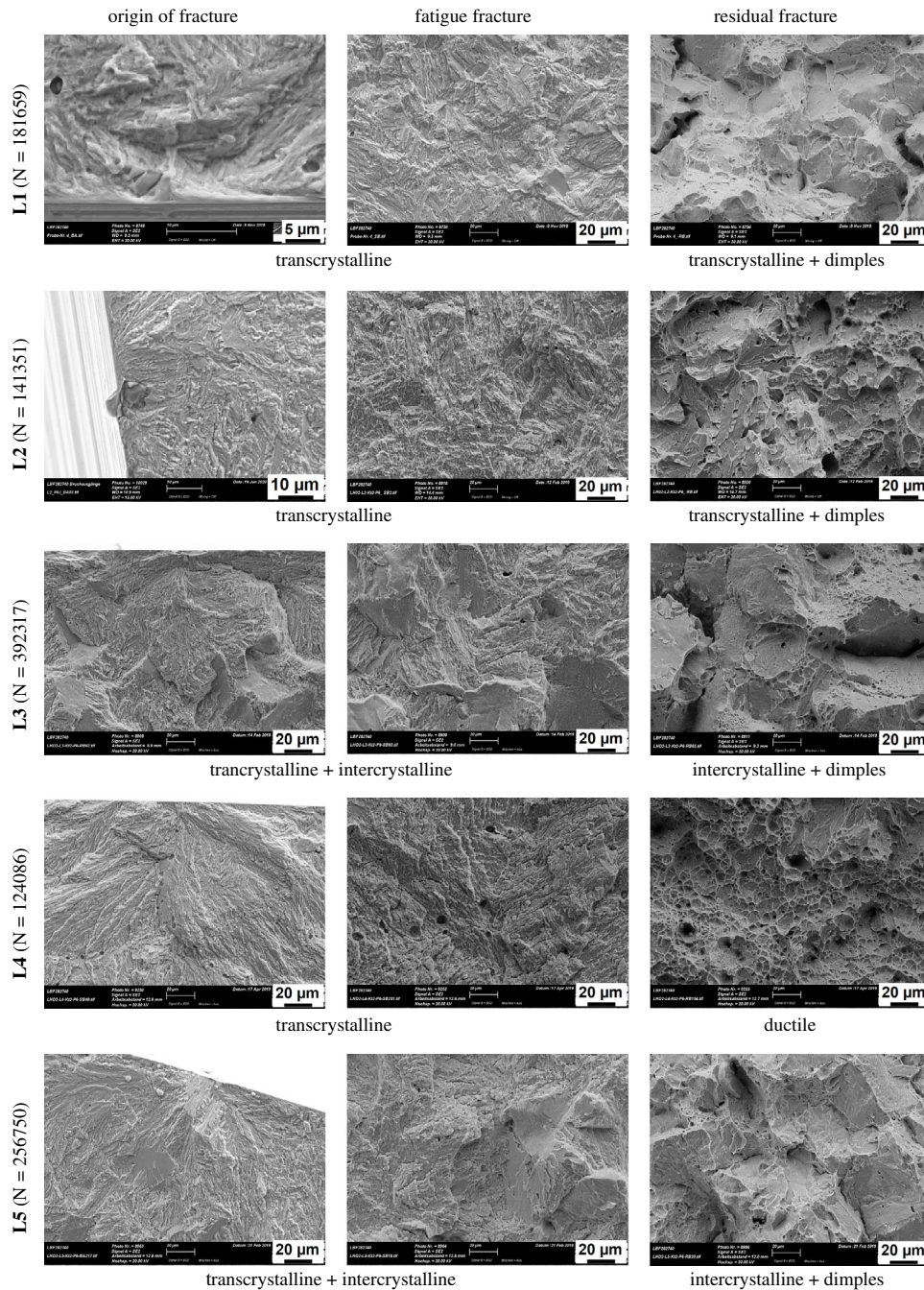
Figure 9. Fatigue strength of notched specimens in the HCF regime of the Q+T steel 42CrMo4,[16] the LHD steel LHD-11,[19] and the alloys L1–L5.[27]

specimens with cycles to failure close to the knee point were analyzed for the alloys L1–L5. The alloys L1 and L2 show a transcrystalline fatigue fracture and the residual fracture is characterized by a transcrystalline overload fracture with dimples (see **Figure 10**). Precipitates are present at the crack initiation location for the alloys L1 and L2 (Figure 10). Transcrystalline and intercrystalline fatigue fracture takes place for the alloys L3 and L5 (Figure 10). No precipitates as crack initiation point could be determined at the origin of fracture. The residual fracture shows an intercrystalline fracture behavior and the amount of dimples is less pronounced for L5 in comparison with L3 (Figure 10). In contrast, alloy L4 shows a purely transcrystalline fatigue fracture and a purely ductile residual fracture (Figure 10). Similar to L3 and L5, the origin of fracture is not located at precipitates.

4. Discussion

The tensile properties of the alloys L1–L5 indicate that tensile strength mainly depends on the carbon content (Figure 5). Increasing carbon content leads to a higher tensile strength. Microalloying elements and grain size seem to play a minor role on the tensile properties of the alloys L1–L5.

In contrast, the Charpy V-notch impact energy seems to depend mainly on the microalloying elements. Alloy L4, which is alloyed with both grain boundary strengthening elements boron and molybdenum, shows the highest Charpy V-notch impact energy of 50 J (Figure 7). Comparison of the alloys L3 and L5 shows that molybdenum effectively increases the impact energy but these alloys still show a relatively low impact energy in comparison with the boron-containing alloys (LHD-11, L1, L2). In the case of the boron-containing alloys, it is necessary that the boron is not bonded to other elements and can diffuse to the grain boundaries for strengthening. Therefore, nitride-forming elements, such as titanium and aluminum, are alloyed, consuming the nitrogen and forming nitrides to keep the boron free.[29–31]

Figure 8. Monotonic yield strengths from initial loading curve and cyclic yield strengths $R*_{p0.2}$ from IST of the Q+T steel 42CrMo4,[16] the LHD steel LHD-11,[19] and the alloys L1–L5.[27]

Figure 10. Secondary electron images of the fracture surfaces of the notched fatigue specimens close to the knee point for the alloys L1–L5.

Therefore, higher boron contents require also the alloying of higher amounts of titanium or aluminum. The alloy LHD-11, with 0.0029 wt% boron, shows a higher Charpy V-notch impact energy than L1, with a boron content of 0.0016 wt% (Figure 7). This leads to the assumption that the Charpy V-notch impact energy increases with increasing boron content. However, alloy L2, which contains 0.0057 wt% boron, shows a lower impact energy than LHD-11. The reason for this is that the titanium content is too low to prevent the formation of boron nitrides, which results in minor grain boundary strengthening and

therefore in a lower Charpy V-notch impact energy. In contrast, alloy L4 is hyperstochiometrically alloyed with aluminum to completely ensure that boron nitride formation is not possible. In addition, investigations reported in the literature have shown that around 0.0030 wt% boron gives a saturation level of grain boundary strengthening,[29] although this cannot be rebutted or confirmed by this study. Nevertheless, boron effectively strengthens the grain boundaries and increases the impact energy. All in all, the Mo–B–Al concept (L4) leads to the best combination of high strength and high Charpy V-notch impact

**ADVANCED
SCIENCE NEWS**

www.advancedsciencenews.com

**steel
research**
international

www.steel-research.de

energy of all the new alloys. In comparison with other forging steels, the Mo–B–Al LHD concept (L4) offers, with a short and simple process route, an outstanding performance regarding high tensile properties and high Charpy V-notch impact energy (**Figure 11**). The cyclic material behavior and the fatigue strength also play an important role in performing a lightweight design. Despite high tensile properties, the reference steel 42CrMo4 shows a low cyclic yield strength of 560 MPa due to cyclic softening (see Figure 8). In contrast, the five alloys L1–L5 show cyclic hardening leading to a high cyclic yield strength of around 1000 MPa (Figure 8). In general, Q+T steels show cyclic softening, PHFP steels shows a cyclically neutral behavior, and TRIP steels, as well as the new LHD alloys, show cyclic hardening (see **Figure 12**a). The values of the cyclic yield strength of the alloys L1–L5 follow a similar trend to the strength values of tensile properties. This indicates a correlation between the cyclic yield strength and the tensile properties. For the alloys L1–L5, it is not clear whether the cyclic yield strength mainly depends
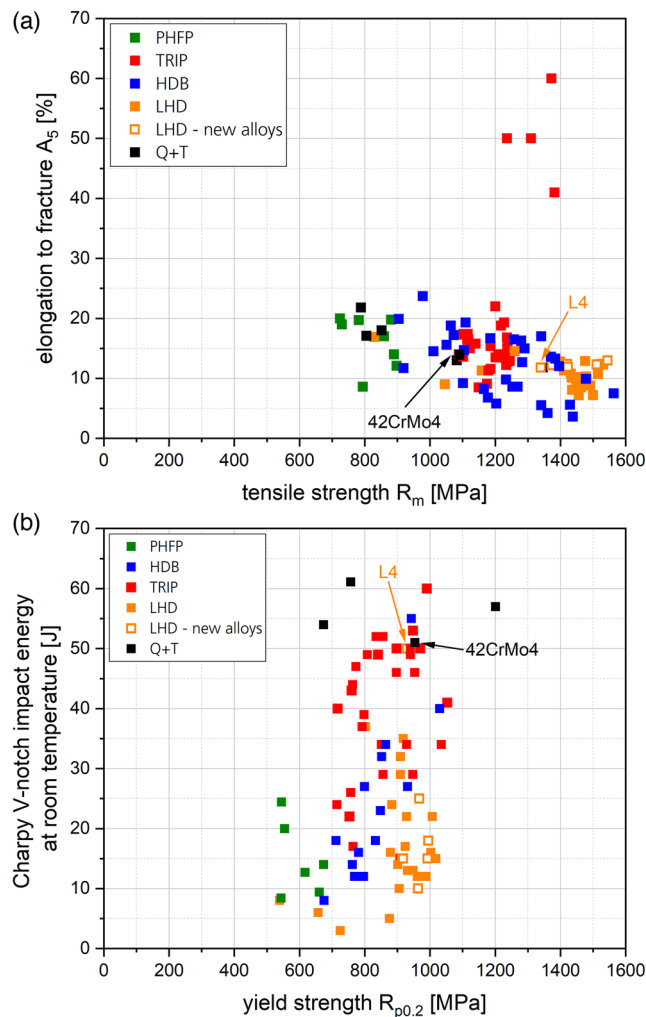
Figure 11. a) Elongation to fracture A_5 versus tensile strength R_m and b) Charpy V-notch impact energy at room temperature versus yield strength $R_{p0.2}$ for different forging steels (PHFP,[4,5] HDB,[7] TRIP,[16] LHD,[19] and Q+T[4,5,16]) and for the new LHD-alloys.[27]
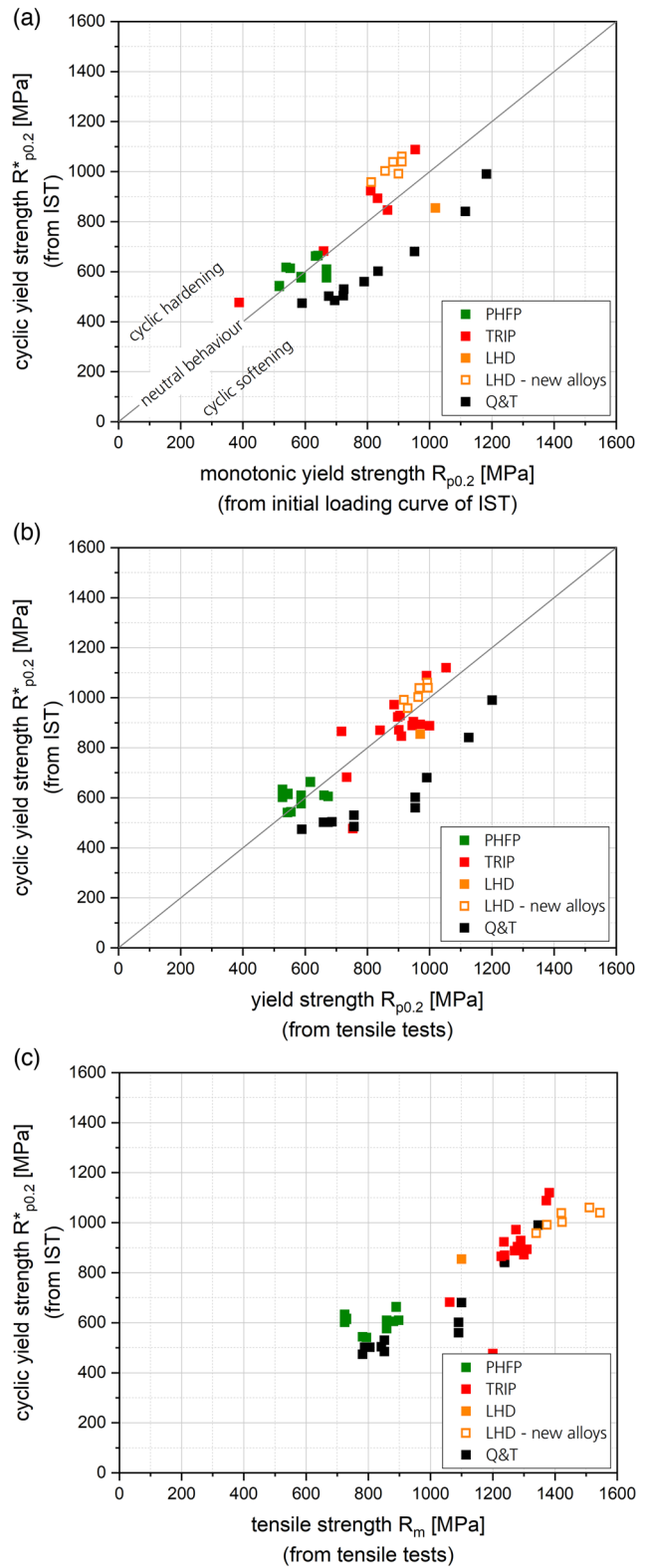
Figure 12. Cyclic yield strength from IST versus a) monotonic yield strength from initial loading curve of IST, b) the yield strength from tensile tests, and c) the tensile strength from tensile tests for different forging steels (PHFP,[4,5] TRIP,[16] LHD,[19] and Q+T[4,5,16]) and the new LHD alloys.[27]

on the yield or on the tensile strength. However, investigations of other forging steels lead to the assumption that the cyclic yield strength correlates well with the tensile strength and less well with the yield strength (see Figure 12b,c).

The alloys L1–L5 also show improved fatigue strength in the HCF regime in comparison with the reference steel 42CrMo4 (Figure 9). No correlation of the fatigue strength in the HCF regime with the tensile properties or the cyclic yield strength could be determined for the alloys L1–L5. However, the alloys that are alloyed with titanium (L1, L2) show a lower fatigue strength in the HCF regime than the alloys without titanium (L3–L5) (see Figure 9). Titanium nitrides are observed in the alloys L1 and L2 and are characterized by a sharp morphology, as reported elsewhere.[28] Therefore, they act as inner notches which favor crack formation under cyclic loading. For alloy L4, small and round aluminum nitrides are observed,[28] but these are not as critical for fatigue crack formation as titanium

nitrides due to their morphology. In general, the fatigue strength depends on the tensile properties of a material (yield strength and tensile strength), as shown in **Figure 13**. However, in detail, the fatigue strength is strongly affected by microstructural defects.[32]

The surface fractures of the notched fatigue specimens of the alloys L1 and L2 indicate that boron effectively strengthens the grain boundaries and prevents intercrystalline fracture (see Figure 10). Due to the significant fraction of intercrystalline fractures for the molybdenum-containing alloys L3 and L5, the effect of molybdenum on the grain boundary strengthening is less pronounced (Figure 10). The addition of 0.5 wt% aluminum in combination with boron and molybdenum (L4) leads to a completely transcrystalline fracture with a ductile residual fracture (Figure 10). A comparable trend, for the alloys L1–L5, is also observed for the fracture behavior of the Charpy V-notch impact energy specimens.[28] Crack initiation takes place at precipitates for the alloys L1 and L2 (Figure 10), explaining the lower reported fatigue strength of these alloys in comparison with the alloys L3–L5. Gramlich et al.[28] showed that titanium nitrides possess a rectangular morphology with sharp edges, whereas aluminum nitrides appear round and cylindrical. Therefore, titanium nitrides seem to favor fatigue crack initiation, leading to a lower fatigue strength.

5. Conclusions

The alloy group of air-hardening martensites offers the best combination of tensile and cyclic properties of the presented forging steels groups (PHFP, HDB, TRIP, Q+T). Further advantages are low alloying, processing and machining costs as well as low CO_2-emissions because additional heat treatments are not necessary.

The following conclusions can be drawn from this study: 1) The cyclic yield strengths correlate with the tensile properties, especially with the tensile strength, which itself depends on the carbon concentration dissolved in the matrix. 2) The fatigue strength in the HCF regime is connected to the size and morphology of the nitrides and is therefore influenced by the nitride-forming elements titanium and aluminum. Titanium nitrides in contrast to aluminum nitrides act as inner notches, negatively affecting the fatigue strength. 3) The prior austenite grain boundary strengthening is also increased under cyclic loading by boron and molybdenum, but the effect of boron is more pronounced. 4) The Mo–B–Al LHD concept offers the best combination of high tensile properties, high impact energy, and high cyclic properties.
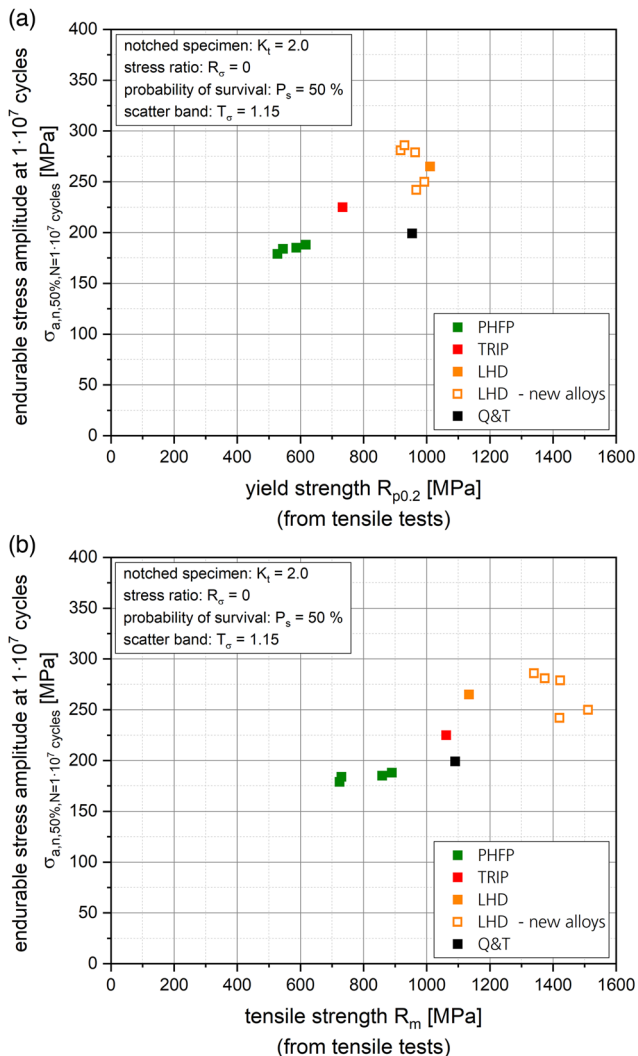
Figure 13. Fatigue strength of notched specimens in the HCF regime versus a) the yield strength from tensile test and b) the tensile strength from tensile tests for different forging steels (PHFP,[4,5] TRIP,[16] LHD,[19] and Q+T[4,5,16]) and for the new alloys.[27]

Conflict of Interest

The authors declare no conflict of interest.

Keywords

forging steels, fracture behavior, martensite, medium manganese steels, tensile and cyclic properties

[1] W. Bleck, M. Bambach, *HTM Heat Treat. Mat.* **2017**, *72*, 6.
[2] W. Bleck, *Werkstoffkunde Stahl für Studium und Praxis*, Verlag Mainz, Aachen, Germany, **2010**.
[3] K.-W. Wegner, *ATZ Automobiltech.* **1998**, *100*, 918.
[4] N. Exel, M. Türk, *Einfluss von Faserverlauf und Gefüge auf die Schwingfestigkeit Warmmassivumgeformter AFP-Stähle*, Final Report, AVIF A 245, Forschungsgesellschaft Stahlverformung e.V. FSV, Hagen **2010**.
[5] M. Wallmichrath, A. Herbert, *Betriebssichere Auslegung von Fahrwerkssicherheitsbauteilen aus AFP-Stahl*, Final Report, IGF-16435 BG, Forschungsgesellschaft Stahlverformung e.V. FSV, Hagen **2013**.
[6] C. Lemaitre, P. Dierickx, *Iron Steel Technol.* **2007**, *4*, 9.
[7] C. Keul, *Ph.D. Thesis*, RWTH Aachen University, December **2012**.
[8] A. Gramlich, T. Schmiedl, presented at MSC Congress, Air-Hardened, Martensitic Forging Steels with Medium Manganese Content, Darmstadt, Germany, September **2018**.
[9] W. Bleck, C. Keul, *Schmiede J.* **2010**, *3*, 42.
[10] E. Erisir, B. Zeislmair, presented at 19th IFC, New Developments for Microalloyed High Strength Forging Steels, Chicago, USA, **2008**.
[11] C. Keul, V. Wirths, *Arch. Civil Mech. Eng.* **2012**, *12*, 119.
[12] C. Keul, M. Urban, *Schmiede J.* **2010**, *9*, 28.
[13] F. Caballero, H. Bhadeshia, *Mater. Sci. Forum* **2003**, *426–432*, 1337.
[14] V. Wirths, R. Wagener, *Adv. Mat. Res.* **2014**, *922*, 813.
[15] V. Wirths, *Ph.D. Thesis*, RWTH Aachen University, October **2016**.
[16] V. Wirths, L. Elek, Schmiedestähle mit verbesserter Betriebsfestigkeit durch verformungsinduzierte Phasenumwandlung, Final Report, IGF-374ZN, Forschungsgesellschaft Stahlverformung e.V. FSV **2014**.
[17] A. Stieben, W. Bleck, *massivUmformung* **2016**, *9*, 50.
[18] A. Stieben, PhD Thesis, RWTH Aachen University, March **2018**.
[19] A. Stieben, *Lufthärtende, duktile Schmiedestähle mit erhöhten Mangangehalten (LHD Schmiedestahl)*, Final Report, AVIF A276, Forschungsgesellschaft Stahlverformung e.V. FSV **2016**.
[20] M. Kuzmina, D. Ponge, *Acta Mater.* **2015**, *86*, 182.
[21] M. Kuzmina, M. Herbig, *Science* **2015**, *349*, 1080.
[22] S. Hwang, J. Morris, *Metall. Trans. A* **1980**, *11*, 1626.
[23] S. Song, R. Faulkner, *Mater. Sci. Eng. A*, **2000**, *12*, 281.
[24] DIN EN ISO 6892-1:2017-02, *Metallic Materials—tensile testing—Part 1: Method of a Test at Room Temperature (ISO 6892-1:2016)*, German Version EN ISO6892-1:2016, Beuth Verlag GmbH, Berlin, https://doi.org/10.31030/2384831.
[25] DIN EN ISO 14556:2017-05, *Metallic Materials—Charpy V-Notch Pendulum Impact Test—Instrumented Test Method (ISO 14556:2015)*, German version EN ISO 14556:2015, Beuth Verlag GmbH, Berlin, https://doi.org/10.31030/2659577.
[26] J. Spindel, E. Haibach, *Int. J. Fatigue* **1979**, *1*, 81.
[27] T. Schmiedl, A. Gramlich, presented at METEC & 4th ESTAD, June **2019**.
[28] A. Gramlich, T. Schmiedl, *Mater. Sci. Eng. A*, **2020**, *784*, 139321.
[29] M. Sharma, I. Ortlepp, *Steel Research Int.* **2019**, *90*, 1900133.
[30] M. Paju, *Ironmak. Steelmak.* **1992**, *19*, 495.
[31] B. Kapadia, *J. Heat Treat.* **1987**, *5*, 41.
[32] U. Zerbst, M. Madia, *Eng. Fail. Anal.* **2019**, *97*, 777.